NOTES AND CORRESPONDENCE

Thunderstorm Electrification Analysis: The Dependence on the Temperature–LWC Diagram

CARLOS M. SCAVUZZO AND GIORGIO M. CARANTI

Facultad de Matemática, Astronomía y Física, Universidad Nacional de Córdoba, Córdoba, Argentina

4 October 1994 and 7 August 1995

ABSTRACT

The dependence on liquid water content (LWC) and temperature (T) of the charge transfer, and in particular its sign, during ice crystal–graupel collisions is a matter of controversy. Some of the laboratory measurements do not agree on the general shape of this function, although they agree on the existence of a critical temperature T_r, above which there is one sign and below which the opposite one. In this paper, the authors carry out a numerical study to investigate the behavior of three charging parameterizations in thunderstorm electrification. This study is carried out on one cloud case study, and a limited set of T–LWC values are present. Surprisingly, the general behavior is the same among the three, despite the distinct differences in the charging diagrams.

1. Introduction

Inside thunderclouds with an important electrical development, aircraft and balloon measurements of the charge on precipitation particles have shown that the integrated charge densities are adequate to account for the observed electric fields (Gaskell et al. 1978; Dye et al. 1986; Weinheimer et al. 1991). It is also basically accepted that the interactions between ice particles in thunderclouds are the main cause for their electrification (Williams 1989).

The charge separated depends on the size and kind of particles colliding. It is also observed that the charge transferred between two ice particles depends mainly on two environmental parameters: temperature (T) and liquid water content (LWC). There are two measured charging versus T, LWC diagrams. One is Takahashi's (1978) result (Fig. 8), and the other is presented by Saunders (1994) (Fig. 1) and Saunders et al. (1991) (Fig. 7). The latter is actually a compilation of their own results, as well as those of Jayaratne et al. (1983), Baker et al. (1987), and Keith and Saunders (1990).

The first diagram was obtained using a rotating rimer at about 9 m s^{-1} inside a cloud chamber. The electric current collected by the rimer was measured while it was hit simultaneously by vapor-grown ice crystals and supercooled water droplets. The temperature was varied in the range (0° to −30°C) and the LWC between 0.01 and 20 g m^{-3}. The mean size of the droplets was 10 μm for low LWCs, increasing to 100 μm for larger LWCs. The LWC was measured by an independent rimer. Although there is some controversy on the meaning of Takahashi's LWC measurements, we are going to use them at face value. The problems arise mainly because there was no compensation in Takahashi's experiment for the ice crystals also collected by the second rimer, which would have resulted in a LWC overestimation. Figure 1 shows a parameterization of only the sign dependence of his diagram of charge. There is a region of negative charging surrounded by positive charging. The negative region covers an area defined by −10°C on the higher temperature side (although there are negative charges scattered above that temperature) and 0.2–4 g m^{-3} along the vertical scale. The large range of LWC and T used by Takahashi makes this diagram important, in spite of the fact that it was taken at a fixed 9 m s^{-1} velocity.

Jayaratne et al. (1983) and Baker et al. (1987) measured charging with LWCs up to 2 g m^{-3}. The impact velocities, 1 m s^{-1}–3 m s^{-1}, were smaller than Takahashi's. Crystal sizes spanned from 30 to 125 μm, while the droplet spectrum ranged from 8 to 30 μm. Joining data from both experiments, the range of temperatures covered was from −5° to −35°C. Saunders et al. (1991) varied LWC systematically while measuring the charge collected by a stationary target. Effective LWCs covered the range of 0.16–1.1. Effective LWC is the product of the actual LWC by the collision efficiency of a graupel placed as a target. It is the water content actually involved in the growth of the target, and it is clearly dependent both on target variables (its

Corresponding author address: Dr. Carlos M. Scavuzzo, FaMAF–UNC, Ciudad Universitaria, 5000 Córdoba, Argentina.
E-mail: scavuzzo@roble.frs.uncor.edu

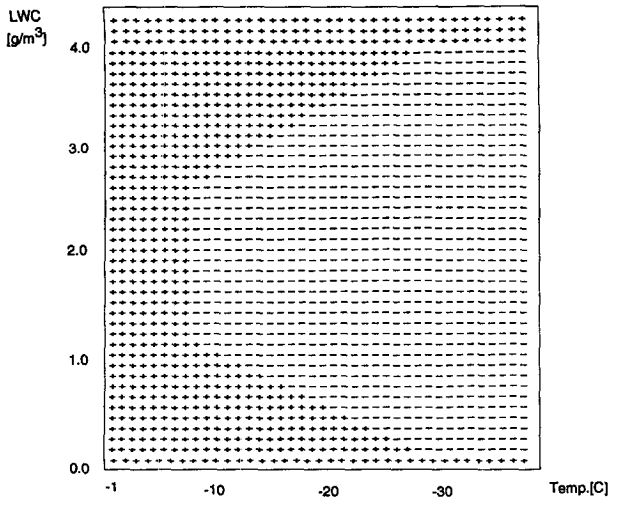

FIG. 1. Takahashi's LWC vs T charging diagram. The "+" symbolizes (LWC, T) points where graupel gets a positive charge. The inverse applies for "−".

size and velocity) and cloud variables (droplet spectrum). Crystal sizes in Saunders et al. (1991) were in a narrow range (100–120 μm), and the impact velocity was 3 m s^{-1}. Figure 2 shows the charging diagram parameterizated by Saunders et al. (1991). The boundary between positive and negative charging is a diagonal line in the temperature range of −10° to −23°C. For each temperature, LWCs below the boundary line result in negative charging. The charging for low LWCs and low temperatures show a positive region inside the negative one.

The two charging diagrams are different, but it is possible to find regions with similar sign predictions. Above −10°C and above 0.2 g m^{-3}, both diagrams predict positive charges to the target. For LWCs lower than 1.1 g m^{-3} and low temperatures, there is an important region where both diagrams assign negative charge. It is important to note that we are comparing effective liquid water content (EW) with LWC. EWs of around 1.1 g m^{-3} in Saunders' diagram would correspond to slightly larger LWCs in Takahashi's diagram. It is not possible to give the exact axis transformation since it involves many parameters, some of which are not available from the respective experiments.

In order to simulate cloud electrification, several numerical models have been developed, using different combinations of electrical and microphysical processes (Helsdon and Farley 1987; Takahashi 1983, 1984). In particular there are numerical cloud electrification models that include only one mechanism in order to test its particular role on cloud-scale processes (Norville et al. 1991; Scavuzzo et al. 1995). The latter studies also show that a mechanism of charge separation, involving only collisions between ice particles, is sufficient to reproduce the most important features of the known thunderstorm electrical structure.

The above comments together with those of Saunders (1994) suggest that the principal difference, between the Saunder's 1991 results and the ones by Takahashi (1978), is the reversal temperature dependence on LWC. Although some explanations can be given for this difference, so far, important questions have not been asked: How relevant are these differences in the experimental results when they are taken into account in a cloud electrification model? Is the electrical structure of a thunderstorm critical to these differences? In this paper we try to answer these questions. Using a numerical cloud electrification model of the electrical structure of the cloud, we present a comparative study of three different parameterizations of the reversal temperature dependence on liquid water contents. It is carried out on a standard cloud that necessarily has a limited set of T–LWC values. In the model only the ice crystals–graupel interaction are considered. The three parameterizations used are based on Manchester's laboratory dataset, on Takahashi's dataset, and an idealized parameterization that has a constant reversal temperature. Also, we present a more detailed discussion of the performance of the model using the Manchester dataset since the model shows some improvements, such as a tridimensional domain and the dependence of the reversal temperature with LWC, with respect to other works (Norville et al. 1991) that also use Manchester results.

2. The model

The numerical model for electrification is kinematic with the cloud fields obtained first from a 3D numerical

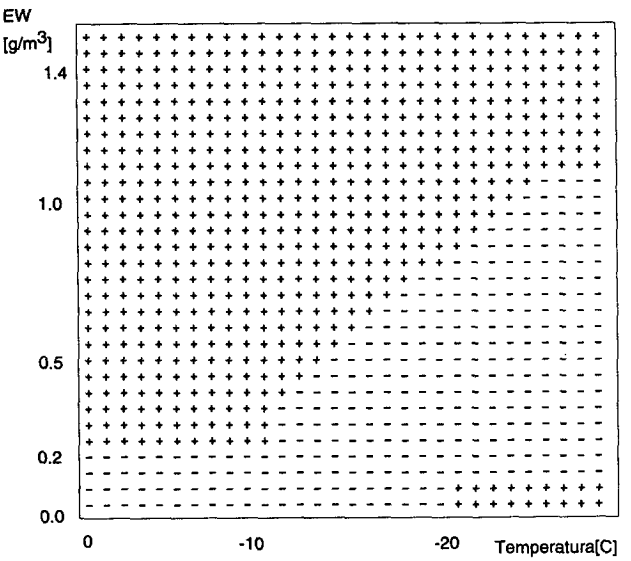

FIG. 2. Saunders's LWC vs T charging diagram. It is important to note that the vertical axis is the EW instead of LWC.

cloud model (Scavuzzo and Castellano 1992), then using those cloud fields, the electrical aspects are incorporated in a manner similar to Scavuzzo et al. (1995). The principal aspects of our cloud model can be found in Scavuzzo et al. (1995). The output of the cloud model used as input in this work simulates an idealized self-consistent case with the purpose of testing our ideas on how the cloud becomes electrified.

As mentioned in the introduction, the only mechanism to be studied in the present work is that of ice crystal–hail collisions. All other possible interactions to fully simulate the electrification of a thundercloud are neglected, that is, ice–water, water–water, ion capture, and induction charging, among others.

In this work the interacting ice particles are described by a discrete spectrum (Takahashi 1984; Norville et al. 1991). The spectrum covers a wide range of sizes in eight categories. In terms of their equivalent diameters they are 1) 10 μm, 2) 30 μm, 3) 50 μm, 4) 100 μm, 5) 250 μm, 6) 500 μm, 7) 1000 μm, and 8) >5000 μm. For each class, two variables are stored in the program, the number concentration and the charge, giving a total of 16 variables to be followed in their evolution.

This is a small number of categories if we compare our work with that of Norville et al., where the same kind of interactions were simulated with 78 categories of ice; however, it will be shown that the most important interactions are those of the spectrum extremes, so it is not totally necessary to include a finer spectrum. Moreover, our model runs on a tridimensional mesh.

The particles do not grow during this electrification test (Latham and Dye 1989). On the other hand, particles of class 8 fall out of the cloud rather fast. In order to keep their number more or less constant, they were replenished; thus, the mature stage of a cloud is simulated. Particles of any class falling below a certain altitude are considered lost.

Basically, the parameterization for the charge separation on each collision follows the Norville et al. (1991) work. The charge (δq) transferred to a large particle (diameter D) in a collision with a smaller particle (diameter d) is the following:

$$\delta q(d, D, l_{wc}, T) = S(T, l_{wc})R(d, D, l_{wc})M(d, D, T),$$

where $S(T, l_{wc})$ determines the sign of the charge transferred, R is a restriction function with values 0 or 1, and M is the magnitude of the charge transferred. The sign function S is a function of the reversal temperature $T_r(l_{wc})$ and is given by

$$S(T, l_{wc}) = -1 \quad T < T_r(l_{wc}),$$

$$S(T, l_{wc}) = 0 \quad T = T_r(l_{wc}),$$

$$S(T, l_{wc}) = 1 \quad T > T_r(l_{wc}).$$

This is another improvement over Norville et al. (1991) since they used a fixed value of $T_r = -15$°C. In the discussion section, the consequences of this crude approximation will be considered. As explained above, in the model three different experimental functions $T_r(l_{wc})$ are used: one with the Manchester's dataset, another using the Takahashi experimental data, and an idealized parameterization with constant reversal temperature that is chosen to be $T_r = -18$°C. In principle, any other value of T_r would serve well for the purpose of comparison. However, this value is representative of the experimental data, at least for water contents of the order 0.5–0.7 g m^{-3}.

As in Norville et al. (1991), the restriction function R determines whether or not the charge process is active. The function R is composed of three step functions on different variables. (a) A step function with a threshold of LWC = 0.05 g m^{-3}. (b) The second step function gives a size threshold of the larger particle, above which it starts riming. This threshold value is set as in Norville et al., $D_r = 400$ μm. (c) The last step function has a different meaning. Differences in surface properties of the colliding particles are important for the charge transfer, as experiments show. Therefore, a parameter is used to separate the "larger" particles growing principally by riming from the "smaller" particles growing by vapor deposition, or by both vapor deposition and riming. This threshold is 1000 μm. This means that in a collision there must be one particle smaller than 1000 μm and one larger than 400 μm.

In order to parameterize the magnitude of the charge transferred, the dependence with the size of the colliding particles given by Keith and Saunders (1990) is used in the present model. Saunders (1994) points out that there is a broad agreement in charge magnitudes between his results and those of Takahashi; therefore, it is reasonable to use Keith and Saunders (1990) results in the model when using Takahashi's sign diagram. It is important to take into account that Manchester data is presented as charge per crystal separation event, whereas Takahashi's data is presented as charge per crystal collision. The separation event probability is defined as the product of the collision and separation probabilities.

The number of collisions between particles in class "i" and "j" per unit volume N_{ij} is calculated following the Scavuzzo et al. (1995) scheme. In that scheme the volume swept by a graupel particle relative to the crystals is calculated, and a random spatial distribution of ice particles on the latter volume is assumed. With this hypothesis, the total number of collisions per unit time and unit volume between particles i and j is given by

$$N_{ij} = \pi R_g^2 E |V_{ti} - V_{tj}| N_i N_j,$$

where N_i is the number density of i particles, R_g is the radius of the larger particle, and E is the efficiency of the process.

On the other hand, the transport equations for the number N_i and charge densities C_i of each class of particle are as follows:

$$\frac{\partial N_i}{\partial t} = -\mathbf{V}\cdot\nabla N_i + V_{\mathrm{Ti}}\frac{\partial N_i}{\partial z} + T_{\mathrm{eddy}} \quad i = 1, 8$$

and

$$\frac{\partial (C_i N_i)}{\partial t} = -\mathbf{V}\cdot\nabla (N_i C_i) + V_{\mathrm{Ti}}\frac{\partial (N_i C_i)}{\partial z} + T_{\mathrm{eddy}} + \left[\frac{\partial (C_i N_i)}{\partial t}\right]_{\mathrm{inter}} \quad i = 1, 8,$$

where $\mathbf{V}$ is the air velocity, T_{eddy} is the artificial viscosity term, and $[\partial(C_i N_i)/\partial t]_{\mathrm{inter}}$ represents the charge source by collisions. These equations are solved using simple first-order finite differences in space and advanced in time. The chosen grid space was 500 m with a total of $32 \times 32 \times 32$ points. Periodic conditions were used for the lateral boundaries. At the top and bottom of the region all variables were taken as zero. All crystals falling through the 0°C isotherm were eliminated in order to account for their melting. A small time step (1 s) was used in order to keep the advection contribution at reasonable values, as concentration gradients can be rather large for some kind of particles. The code used for the cloud model and for the electrification model was written in Fortran, and both programs run on a NeXT computer.

3. Initial conditions

The cloud considered in this simulation had grown for 14 min. It is a simple, almost symmetric cell, although the model can also simulate asymmetric cases well. The symmetric cell was preferred for this initial electrification test in order to facilitate the interpretation of results. Its updraft region is 4 km in diameter reaching 25 m s^{-1} vertical air velocity. The cloud base and 0°C altitudes are 2 km and 3.5 km, respectively. The ground temperature is 28°C. Figure 3a shows a horizontal cut of the wind field at 6-km altitude. At this level there is still some convergence in the central region and a stronger divergence at the periphery. The contours shown indicate vertical upward velocities reaching 25 m s^{-1} at this time. Figure 3b presents contour plots of effective liquid water contents (70% of LWC) for the central part of the cloud on a vertical plane.

With respect to the chosen initial particles distribution in height, it was preferable to use exponential laws so that the crystal concentration increased with height while the concentration of large precipitation particles decreased. Therefore, in the center of the domain, all classes were made to follow a law of the form Ae^{Bz}, where z is the altitude and A and B are parameters given according to the class number. Also, on each horizontal plane the initial particle concentration is made to decrease toward the boundary following LWC.

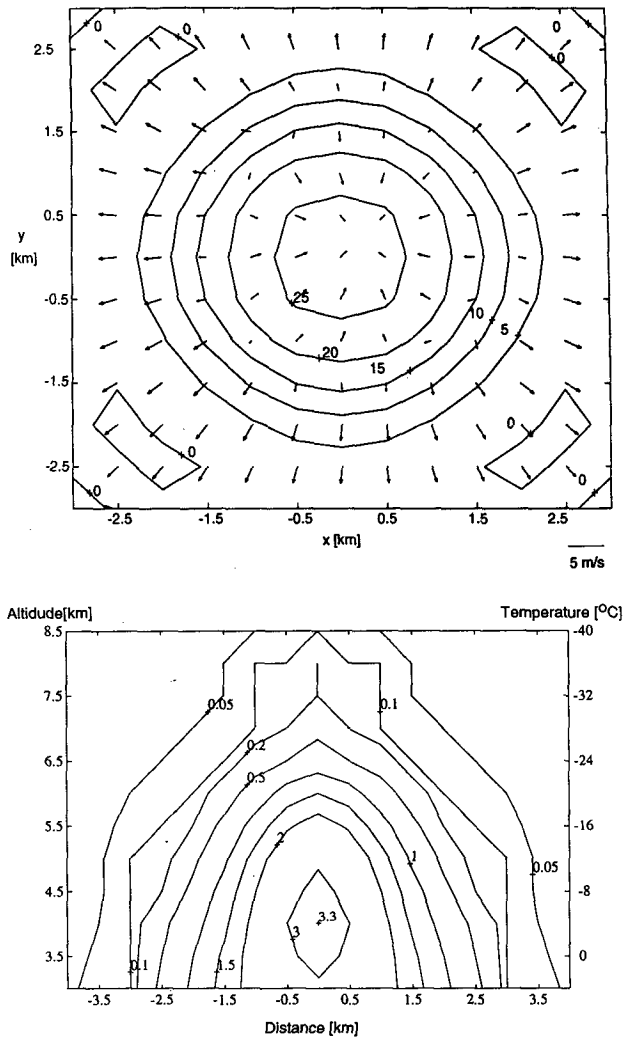

FIG. 3. (a) Cross section of the wind field through the horizontal plane at $Z = 6$ km. Vectors show the horizontal winds, and contours refer to vertical velocity in m s^{-1}. (b) Contour plots of EW in g m^{-3} for the X–Z plane through the center of the cloud.

Classes 1–3 (the cloud ice) have an associated $B > 0$, so their concentration increases with height up to a saturation point from where they stay constant to the top of the cloud. For classes 4–8 (the precipitation) $B < 0$, so they are less numerous aloft (Pruppacher and Klett 1978). The size distribution can now be calculated in different ways. If we use, for example, the Marshall and Palmer relation, the maximum concentrations obtained were as follows: in the upper region for the smaller particles of 700 L^{-1} for 10 μm (category 1), 100 L^{-1} for 30 μm (category 2), and 70 L^{-1} for 50 μm (category 3); and in the lower region for the larger particles of 10 L^{-1} for 100 μm (category 4), 6 L^{-1} for 250 μm (category 5), 5 L^{-1} for 500 μm (category 6),

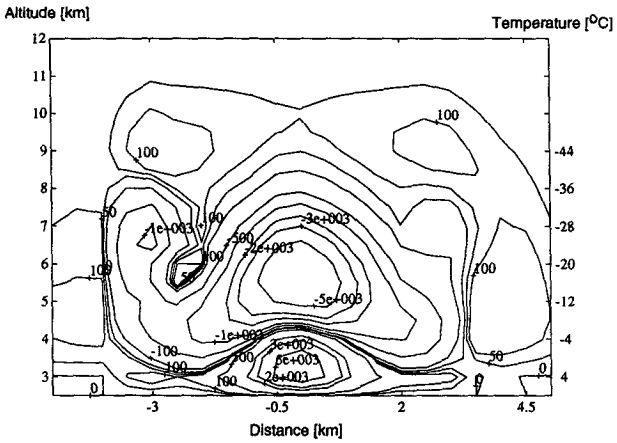

FIG. 4. Contour plots of charge density in fC L^{-1} for the $X-Z$ plane through the center of the cloud at three min. These results are obtained using Takahashi's dataset.

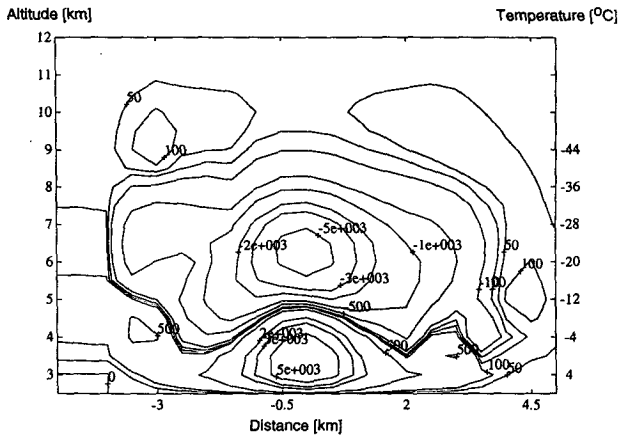

FIG. 5. As in Fig. 4 but using the Manchester dataset.

2 L^{-1} for 1000 μm (category 7), and 0.5 L^{-1} for particles >5000 μm (category 8). Figure 7 (see section 4) shows histograms of described particle concentrations at two altitudes in the cloud. Other histograms showing variations in these concentrations will be presented in the next section. The above simple estimation seemed to be reasonable for a thunderstorm; therefore, it was used to initiate the model, and all particles started the run with zero charge.

4. Results

Figure 4 presents contour plots of charge density for the central part of the cloud on a vertical plane, three min after the beginning of the electrification process. This simulation is run by using Takahashi's experimental dataset. The charge distribution is of a tripolar nature with a localized lower positive charge center with charge densities of about of 5000 fC L^{-1} (femtocoulombs per liter), a middle negative center with charge densities of about -6000 fC L^{-1}, and a stratified upper positive distribution with charge densities of about 100 fC L^{-1}. The charge stratification suggests the presence of a widespread positive anvil. It is interesting to note the complexity of the charge distribution, which is impossible to find in nontridimensional models. This tripolar structure is clearly compatible with the general thundercloud description given by Williams (1989). The upper positive charge is overhanging on the sides, as if it were trying to surround the negative zone. The latter shows high concentration in the center, decaying to a negative horizontal strata toward the sides. The lower positive pocket is completely immersed in a negative environment. This electrical structure is approximately the same found by Scavuzzo et al. (1995), using a model that employs only Avila and Caranti's experimental dataset on ice spheres–graupel collisions (Caranti et al. 1991).

As shown in Fig. 4, Fig. 5 presents contour plots of charge density for the central part of the cloud on a vertical plane, 3 min after the beginning of the electrification process. In this case the simulations were carried out using Manchester's experimental dataset about the dependence of the reversal temperature with the liquid water. The charge distribution is also of a tripolar nature. Now, the lower positive charge center is more extended vertically, reaching 5.5 km instead of the 4.5 km of Fig. 4. The maximum charge density for this zone is about of 5000 fC L^{-1}. The middle negative center has roughly -5000 fC L^{-1} and it is also upwardly displaced by about 0.5 km. The charge densities on the upper positive region are about 50 fC L^{-1}. Clearly, the general appearance as well as the actual values are very similar in these two cases.

The results using the parameterization of fixed reversal temperature is shown in Fig. 6. The cut is taken through the central part of the cloud, and the time of

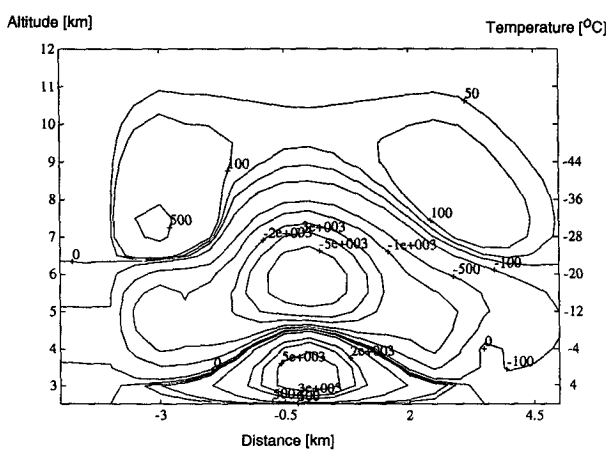

FIG. 6. As in Fig. 4 except using the model with a constant reversal temperature (−18°C).

evolution is the same as in previous figures. Notice that the electrical structure is also of a tripolar nature. Charge magnitudes and charge center locations are similar to the previous cases.

Since the electrical models use an externally imposed initial crystal spectra, one interesting question is how critical the results are to these crystal spectra used to initiate the model. Figures 7a and 7b show the concentration histograms used in the runs of Figs. 4–6 for the lower and upper regions, respectively. Figures 8–10 show three other concentration histograms used to initiate the model, this time using only the Manchester charging diagram. The maximum number of crystals diminishes from 700 L^{-1} in the original to 500, 300, and 100 L^{-1} for Figs. 8–10, respectively. Also, for these extra runs, the large particles concentration is steeper. Particles classes 4–6 are almost constant, but

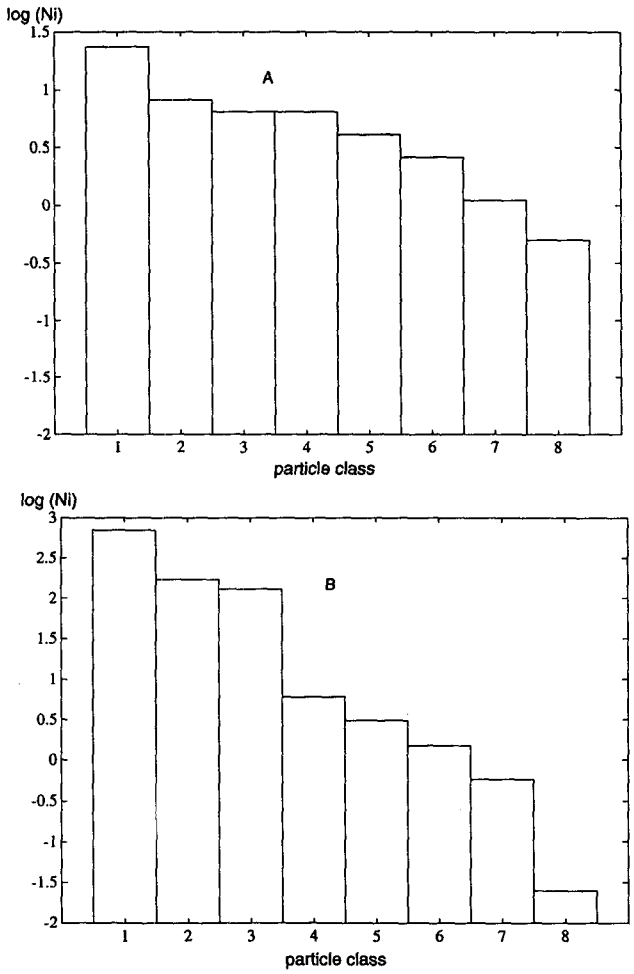

FIG. 7. Particle spectra (at maximum concentration of 700 L^{-1}) used in the initial model runs for the three parameterizations (Figs. 4–6). Axis X corresponds to ice particle size class (see text). Axis Y is number per liter on a logarithmic scale. (a) At 3.5-km altitude (500 m above freezing level). (b) At 8.5-km altitude (1000 m below the cloud top).

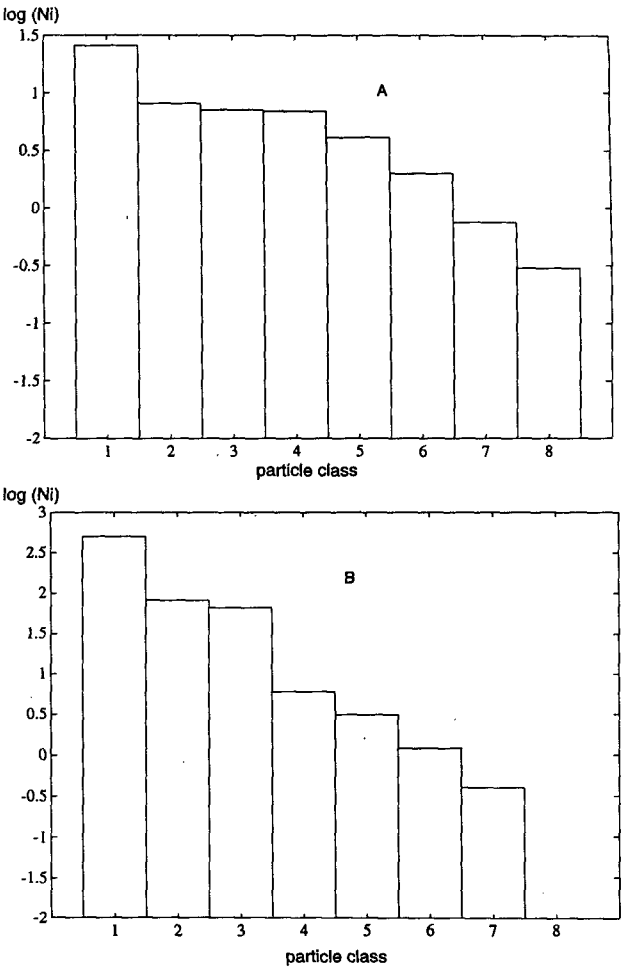

FIG. 8. Different particle distributions used to carry out sensitivity tests. As in Fig. 7 except for maximum concentrations of 500 L^{-1} with fewer large particles (see text).

class 8 changes the concentration from 0.5 to 0.3 and 0.15 L^{-1} for the first two cases, and for the last, the slope is made stepper by changing the concentration of the other sizes. The above figures also show a variation in the height distribution.

Figures 11–13 present contour plots of charge density for the central part of the cloud on a vertical plane, 3 min after the beginning of the charging process using the spectra presented in Figs. 8–10 respectively. We can see that the general structure is maintained and that the charge density maximum changes but is of the same order as the one obtained in the original run. Of course, we could be more specific and we could run tests in order to identify which particles are electrically more important for the Manchester case. We think these tests are out of the scope of this work. Nevertheless, the above test runs help us notice that maximum charges seem to depend mostly on particles classes 6–8 and that lowering the number of crystals does not bring

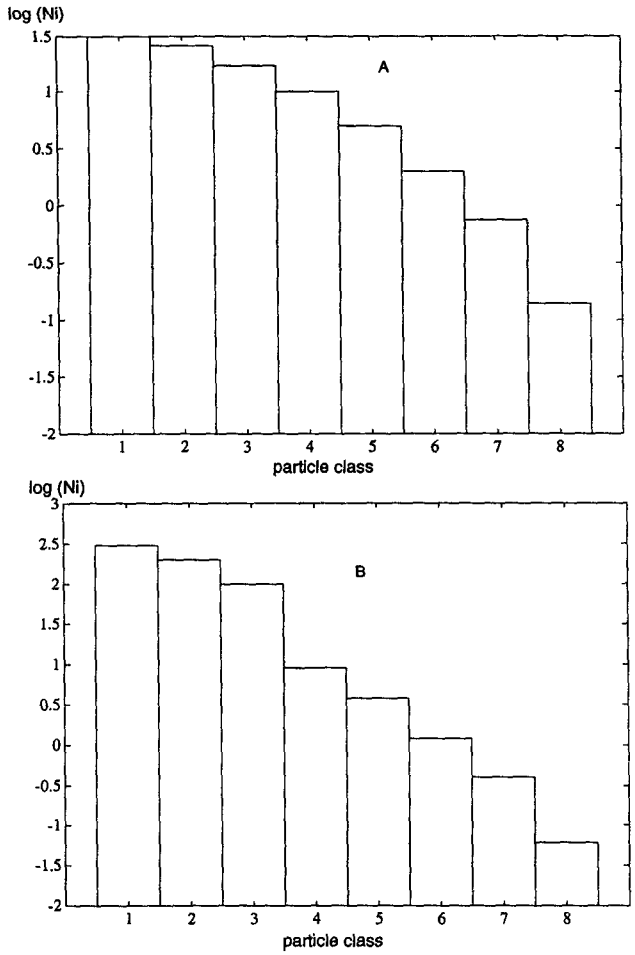

FIG. 9. As in Figs. 7 and 8 except for maximum concentrations of 300 L^{-1} with fewer large particles (see text).

about important changes. Obviously, our spectra tests do not cover the entire range of possibilities for distributions of crystals encountered in actual clouds (which are not precisely known), but we believe that it is an important reliability test to the results and conclusions from this work.

These results are important in two aspects. First, the structure given by the polarity, height of charge centers, order of magnitude, and spatial distribution of the charge, are not critically dependent of the particle spectrum, at least within reasonable limits. Therefore, the results presented in Figs. 4–6 can be considered as representative of what should be expected if a measured spectrum were used. Second, the fact that the electrification shown in Figs. 4 and 5 seems large, perhaps by a factor of 3 or 4, should not be considered as a failure of the mechanism, since this factor is compensated with relatively small variations of the particle spectrum. Therefore, the results should be considered to be representative of the behavior of the system and the orders of magnitude.

5. Discussion and conclusions

As mentioned above, an important and still unanswered question is whether or not the apparently important differences in the experimental charge versus T–LWC diagrams obtained by the Manchester Group and by Takahashi are relevant in the formation of the electrical structure of a storm.

We believe that the results shown in Figs. 4 and 5 are conclusive in this respect. Both the electrical structure, with charge densities differing in less than 10%, and the charge center positions within less than one kilometer tells us that the differences are not being propagated to the large-scale electrification in the same proportion. This is right at least for the subset of the parameters T–LWC involved in the cloud studied. What is even more surprising is that a rough approximation, such as the fixed reversal temperature, still gives believable results.

Clearly, with both more numerical studies with improved models and different kinds of thunderstorms,

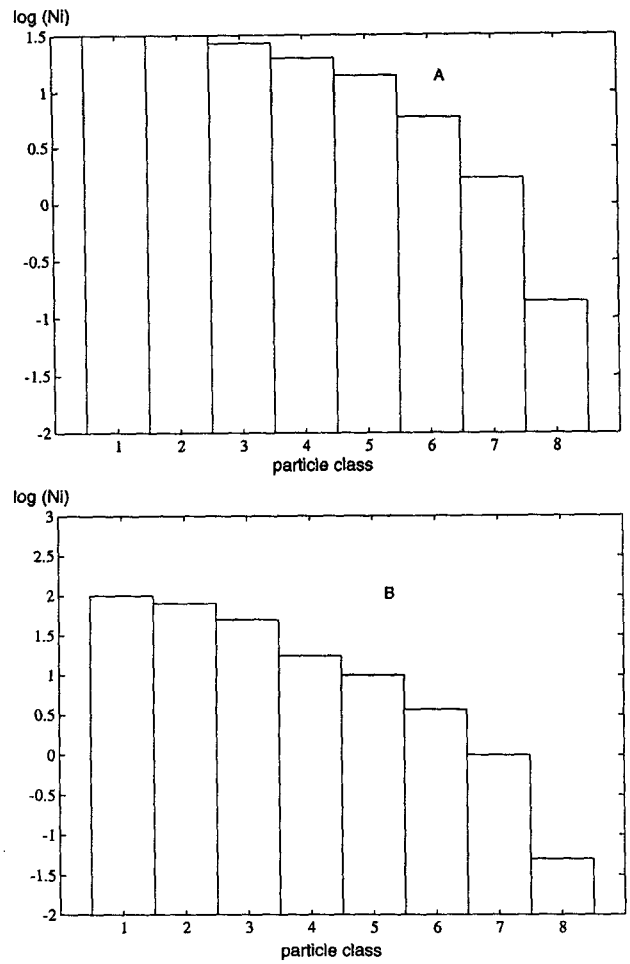

FIG. 10. Additional particle distribution histograms. As in Fig. 7 except for maximum concentrations of 100 L^{-1} (see text).

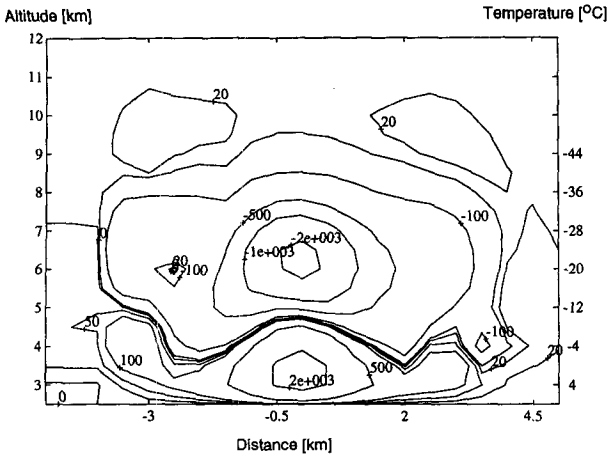

FIG. 11. Electrification results obtained using Manchester data and the particle spectra from Fig. 8.

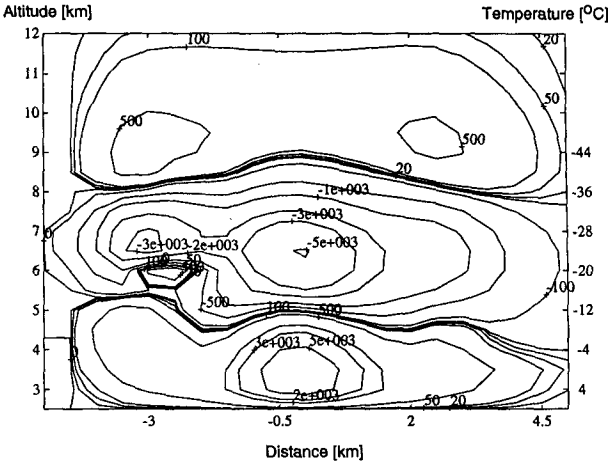

FIG. 13. Electrification results obtained using Manchester data and the particle spectra from Fig. 10.

perhaps covering other regions of the T–LWC diagram, the discussion about which charge diagram is the "correct one" should continue in spite of the present results.

It is important to note that the model is run only until the electric field is strong enough to produce a discharge, a phenomenon not parameterizated in the model. Although three min may seem a short time, it should be kept in mind that we use a mature cell to model the electrification. In a complete coupled model there is the need to wait for the particles to grow. In a way, we are simulating the period between the appearance of a strong echo and the first lightning, or perhaps the period between lightnings.

Generally, when the precipitative mechanisms of cloud electrification are studied, the dynamical aspects of the cloud are taken as a secondary factor (e.g., one-dimensional models, Norville et al. 1991; Latham and Dye 1989). That the results with the three parameterizations modeled and the different initial spectra of crystals are similar in the charge distributions and magnitudes can be interpreted as a confirmation that the dynamical situation of the cloud plays a very important role in this precipitative mechanism of thunderstorm electrification as well. Then, the dynamics aspect must be carefully taken into account when studies of cloud electrification are carried out.

Results shown in Fig. 14 could be used to elaborate an explanation of the similarities in the three parameterization results. The contour plots, on a vertical cut through the central part of the cloud, represent the charge separated at each grid location along the three min using the Manchester data. The maximum charge is generated at the central part of the cloud, around the

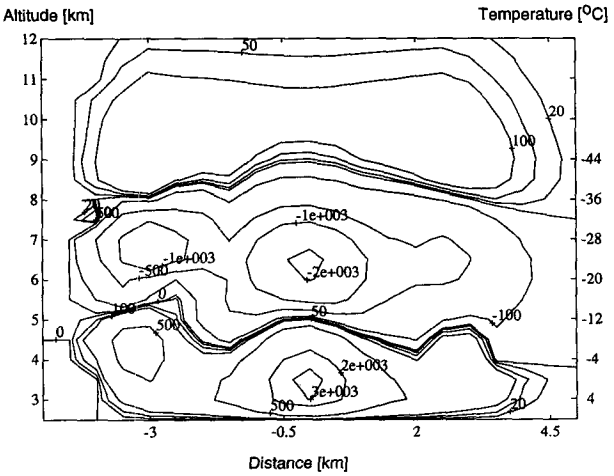

FIG. 12. Electrification results obtained using Manchester data and the particle spectra from Fig. 9.

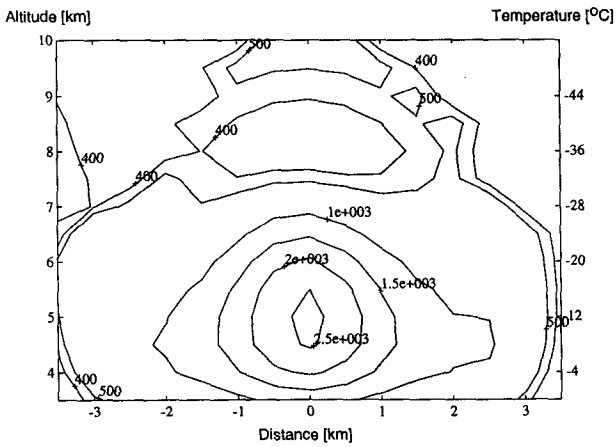

FIG. 14. Contour plots of charge density separated at each location after 3 min, in fC L^{-1}, for the vertical plane through the center of the cloud, using Manchester data.

updraft, between altitudes of 3 and 7 km, corresponding to isotherms of 0° and −30°C, with effective liquid water contents between 2.5 and 3.5 g m^{-3} in the lower part, and less than 1.5 g m^{-3} above 5.5 km. Given these ranges and looking up the T–LWC charge diagrams, it is clear that at lower parts of the cloud graupel or hail would get positive charging for both datasets. The same happens above 5.5 km; both parameterizations would result in negative ice precipitation particles.

The positions, and the magnitude, of the charge center are the result of a dynamic process. The small difference in charge center locations originates in the altitude of the change of sign, which is lower for Takahashi's predictions than for Saunders's. This fact is reflected in the electrical structure. A similar situation occurs for the parameterization independent of LWC.

Summarizing, since in clouds, for temperatures lower than −25°C, the liquid water is frequently lower than 1.5 g m^{-3}, both experimental datasets will predict graupel acquiring negative charge; on the other hand, around the middle of a horizontal plane in the lower part of the cloud with temperatures higher than −12°C, the liquid water contents are usually larger than 0.5 g m^{-3}, and both T–LWC charge diagrams predict the acquisition of positive charge. Therefore, if these are the principal regions of charge generation, it is reasonable to expect a similar electrical structure of the cloud for both parameterizations. Clearly, the other regions of the cloud, where the parameterizations produce different results, are less important for the charge generation, as showed in Fig. 14. With the same arguments, the detailed electrical structure obtained can be explained. In fact, in the upper portions of the cloud, the small particles charge positively, being carried upward to form the positive anvil. In the lower part of the cloud, graupel charge positively, while the smaller particles charge negatively and are also carried upward. These particles, together with the negative graupel falling from above, form the main negative middle center. The lower positive center results mainly from graupel falling from the central region. Although we do not show them, the individual particle charges predicted by the model confirm the above description. Modeling a different mechanism, Scavuzzo et al. (1995) found similar individual charge distributions to those of the present work and discussed these kinds of results, comparing them with in situ measurements.

It is important to note that when we used the Manchester model we included an event probability of 90% equal for all the collisions. It is clear that this is a point that must be improved in every model (particularly in ours), and so far it has not been correctly parameterizated. For some collisions, 90% is larger than the actual value; therefore, we can be sure that if a more realistic parameterization were included, the magnitudes for the Manchester case would be smaller. In spite of all this, we think that the charge values we are obtaining are about right because the associated electric fields are close to the in situ measurements. A possible explanation is that the large particles play a very important role, and for them the event probability is necessarily large.

In spite of some criticisms found in the literature, an important conclusion from the present study is that the electrification generated using the Manchester data is reasonable. Moreover, the tests lowering particle numbers, and perhaps a more correct event probability, would make it even more reasonable.

Although our results seem to be conclusive, we believe that they should be reexamined with more complete numerical models that we cannot run, due to our present computational limitations. Also, it must be borne in mind that our study includes only one case; other meteorological situations covering a more complete set of data from the T–LWC diagram must be done for a generalization of our conclusions. In addition, it should be considered that the ultimate test for any model comes from the adequate description of actual "in situ" electrical thunderstorm data.

Acknowledgments. Thanks to María Inés Pistorio for help with the manuscript. This work was supported by the Consejo Nacional de Investigaciones Científicas y Técnicas, and CONICOR, Argentina.

REFERENCES

Baker, B., M. B. Baker, E. R. Jayaratne, J. Latham, and C. P. R. Saunders, 1987: The influence of diffusional growth rate on the charge transfer accompanying rebounding collisions between ice crystals and hailstones. *Quart. J. Roy. Meteor. Soc.*, **113,** 1193–1215.

Caranti, G. M., E. E. Avila, and M. A. Ré, 1991: Charge transfer during individual collisions in ice growing from vapor deposition. *J. Geophys. Res.*, **96,** 15 365–15 375.

Dye, J. E., and Coauthors, 1986: Early electrification and precipitation development in a small isolated Montana cumulonimbus. *J. Geophys. Res.*, **91,** 1231–1247.

Gaskell, W., A. J. Illingworth, J. Latham, and C. B. Moore, 1978: Airborne studies of electric fields and the charge and size of precipitation elements in thunderstorm. *Quart. J. Roy. Meteor. Soc.*, **104,** 447–460.

Helsdon, J. H., and R. D. Farley, 1987: A numerical modeling study of a Montana thunderstorm: 2. Model results versus observations involving electrical aspects. *J. Geophys. Res.*, **92,** 5661–5675.

Jayaratne, E. R., C. P. R. Saunders, and J. Hallett, 1983: Laboratory studies of the charging of soft hail during ice crystals interactions. *Quart. J. Roy. Meteor. Soc.*, **109,** 609–630.

Keith, W. D., and C. P. R. Saunders, 1990: Further laboratory studies of the charging of graupel during ice crystal interactions. *Atmos. Res.*, **25,** 445–464.

Latham, J., and J. E. Dye, 1989: Calculations on the electrical development of a small thunderstorm. *J. Geophys. Res.*, **94,** 13 141–13 144.

Norville, K., M. Baker, and J. Latham, 1991: A numerical study of thunderstorm electrifications: Model development and case study. *J. Geophys. Res.*, **96,** 7463–7481.

Pruppacher, H. R., and J. D. Klett, 1978: *Microphysics of Clouds and Precipitation.* Reidel, 712 pp.

Saunders, C. P. R., 1994: Thunderstorm electrification laboratory experiments and charging mechanism. *J. Geophys. Res.*, **99,** 10 773–10 779.

——, W. D. Keith, and R. P. Mitzeva, 1991: The effect of liquid water on thunderstorm charging. *J. Geophys. Res.*, **96,** 11 007–11 017.

Scavuzzo, C. M., and N. E. Castellano, 1992: Simulación numérica de procesos atmosféricos. Parte I: modelo de nube. *Metodos Numéricos para el cálculo y diseño en ingeniería,* **8,** 417–426.

——, E. E. Avila, G. M. Caranti, 1995: Cloud electrification by fracture in ice–ice collisions. *Atmos. Res.*, **37**(4), 325–344.

Takahashi, T., 1978: Riming electrification as a charge generation mechanism in thunderstorms. *J. Atmos. Sci.*, **35,** 1536–1548.

——, 1983: A numerical simulation of winter cumulus electrification. Part 1: Shallow cloud. *J. Atmos. Sci.*, **40,** 1257–1280.

——, 1984: Thunderstorm electrification—A numerical study. *J. Atmos. Sci.*, **41,** 2541–2558.

Weinheimer, A. J., J. E. Dye, D. W. Breed, M. P. Spowart, J. L. Parrish, T. L. Hoglin, and T. C. Marshall, 1991: Simultaneous measurements of the charge, size and shape of hydrometeors in an electrified cloud. *J. Geophys. Res.*, **96,** 20 809–20 829.

Williams, E. R., 1989: The tripole structure of thunderstorm. *J. Geophys. Res.*, **94,** 13 151–13 167.